Published OnlineFirst August 24, 2017; DOI: 10.1158/1535-7163.MCT-17-0241

Cancer Biology and Translational Studies

Molecular Cancer Therapeutics

The Selective Tie2 Inhibitor Rebastinib Blocks Recruitment and Function of Tie2^{Hi} Macrophages in Breast Cancer and Pancreatic Neuroendocrine Tumors

Allison S. Harney[1,2,3,4], George S. Karagiannis[1,3,4], Jeanine Pignatelli[1,4], Bryan D. Smith[5], Ece Kadioglu[6], Scott C. Wise[5], Molly M. Hood[5], Michael D. Kaufman[5], Cynthia B. Leary[5], Wei-Ping Lu[5], Gada Al-Ani[5], Xiaoming Chen[1,4], David Entenberg[1,3,4], Maja H. Oktay[1,3,7], Yarong Wang[1,3,4], Lawrence Chun[8], Michele De Palma[6], Joan G. Jones[1,3,7,9], Daniel L. Flynn[5], and John S. Condeelis[1,3,4]

Abstract

Tumor-infiltrating myeloid cells promote tumor progression by mediating angiogenesis, tumor cell intravasation, and metastasis, which can offset the effects of chemotherapy, radiation, and antiangiogenic therapy. Here, we show that the kinase switch control inhibitor rebastinib inhibits Tie2, a tyrosine kinase receptor expressed on endothelial cells and protumoral Tie2-expressing macrophages in mouse models of metastatic cancer. Rebastinib reduces tumor growth and metastasis in an orthotopic mouse model of metastatic mammary carcinoma through reduction of Tie2^{+} myeloid cell infiltration, antiangiogenic effects, and blockade of tumor cell intravasation mediated by perivascular Tie2^{Hi}/Vegf-A^{Hi} macrophages in the tumor microenvironment of metastasis (TMEM). The antitumor effects of rebastinib enhance the efficacy of microtubule inhibiting chemotherapeutic agents, either eribulin or paclitaxel, by reducing tumor volume, metastasis, and improving overall survival. Rebastinib inhibition of angiopoietin/Tie2 signaling impairs multiple pathways in tumor progression mediated by protumoral Tie2^{+} macrophages, including TMEM-dependent dissemination and angiopoietin/Tie2-dependent angiogenesis. Rebastinib is a promising therapy for achieving Tie2 inhibition in cancer patients. *Mol Cancer Ther; 16(11); 2486–501. ©2017 AACR.*

Introduction

The angiopoietin (Ang)/Tie2 kinase signaling pathway is a pivotal angiogenic signaling axis in endothelial cells (1, 2), linked with poor outcome and recurrence in cancer patients (3, 4). Ang/Tie2 signaling is central to the initiation of angiogenesis through vascular remodeling by disrupting endothelial cell interactions. While Ang1 is a Tie2 agonist and has a higher binding affinity to Tie2 than Ang2, Ang2 can act as a context-dependent agonist, although initially described as a Tie2 antagonist (5). Thus, the Ang/Tie2 kinase signaling pathway is an attractive antivascular target (1, 2).

Tie2 is also expressed on a subset of proangiogenic macrophages (i.e., Tie2^{+} macrophages) that are involved in tumor angiogenesis and lymphangiogenesis, as well as in cancer cell intravasation and metastasis (6–11). While antivascular agents (such as bevacizumab and other Vegf-A pathway inhibitors) have shown efficacy in decreasing tumor angiogenesis and disease burden in both preclinical and clinical settings (12, 13), one of the mechanisms of tumor resistance or recurrence after antiangiogenic therapy has been attributed to tumor-infiltrating myeloid cells in response to cell death and hypoxia after vascular regression (14). Of note, Tie2^{+} macrophages are involved in supporting angiogenesis during antiangiogenic therapies (2, 15). Thus, the Ang/Tie2 axis has become an attractive target for inhibiting protumoral functions of Tie2^{+} myeloid cells.

Recently, the paracrine interactions between tumor cells and associated stromal cells, such as fibroblasts, mesenchymal stem cells, and myeloid-derived immune cells among others, have been implicated in a form of transient drug resistance, which has been termed as "environment-mediated drug resistance" (EMDR; refs. 16–18). In particular, tumor-associated macrophages (TAM)

[1]Department of Anatomy & Structural Biology, Albert Einstein College of Medicine, New York, New York. [2]Department of Radiology, Albert Einstein College of Medicine, New York, New York. [3]Integrated Imaging Program, Albert Einstein College of Medicine, New York, New York. [4]Gruss-Lipper Biophotonics Center, Albert Einstein College of Medicine, New York, New York. [5]Deciphera Pharmaceuticals, LLC, Waltham, Massachusetts. [6]ISREC, School of Life Sciences, École Polytechnique Fédérale de Lausanne (EPFL), Lausanne, CH-1015, Switzerland. [7]Department of Pathology Albert Einstein College of Medicine, New York, New York. [8]Emerald Bio, Bainbridge Island, Washington. [9]Department of Epidemiology & Population Health, Albert Einstein College of Medicine, New York, New York.

Note: Supplementary data for this article are available at Molecular Cancer Therapeutics Online (http://mct.aacrjournals.org/).

A.S. Harney and G.S. Karagiannis shared first authorship of this article.

Corresponding Authors: John S. Condeelis, Albert Einstein College of Medicine, 1301 Morris Park Avenue, Price 220 Bronx, NY 10461. Phone: 718-678-1126; Fax: 718-678-1128; E-mail: John.Condeelis@einstein.yu.edu; Daniel L. Flynn, Deciphera Pharmaceuticals, LLC, 500 Totten Pond Road, 6th Floor, Waltham, MA 02451. E-mail: dflynn@deciphera.com

doi: 10.1158/1535-7163.MCT-17-0241

Published OnlineFirst August 24, 2017; DOI: 10.1158/1535-7163.MCT-17-0241

not only promote cancer growth, cancer cell survival, and motility (7, 19–23), but can limit the efficacy of the tumor response to chemotherapy or radiotherapy (24–28). Tie2$^+$ macrophages are known to be proangiogenic, prometastatic, and immunosuppressive in the tumor microenvironment (2, 15, 22, 29). In preclinical studies of mammary carcinoma, Ang2 blockade impeded the association of Tie2$^+$ macrophages with the nascent tumor vasculature, thereby suppressing their proangiogenic activity (8) and their prometastatic potential (8, 30).

In mammary carcinoma, cancer cell intravasation and dissemination occur at microanatomical structures on blood vessels of the tumors, called Tumor MicroEnvironment of Metastasis (TMEM). Each functional TMEM is composed of three different cell types in direct physical contact: a tumor cell expressing the actin-regulatory protein Mammalian-enabled (Mena), a perivascular Tie2^{hi}/Vegf^{hi} macrophage, and an endothelial cell (7, 31). TMEM sites have been identified in mouse and human mammary carcinomas, and their density correlates with metastatic outcome in breast cancer patients (32–34). High-resolution intravital imaging (IVI) of murine primary breast tumors revealed that TMEM sites induce local and transient dissociation of endothelial cell junctions through which migratory cancer cells intravasate and disseminate to secondary sites (7). TMEM-dependent vascular permeability is particularly localized and is mediated by vascular endothelial growth factor-A (Vegf-A) release from the TMEM-bound Tie2^{hi}/Vegf^{hi} macrophage (7).

Biologics that inhibit Ang/Tie2 signaling have been developed, notably angiopoietin-sequestering biologics such as the dual Ang1/Ang2 peptibody AMG-386 (trebananib) and the Ang2-specific monoclonal antibodies MEDI3617 and LC06 (35, 36). In clinical studies, angiopoietin-sequestering biologics increase progression-free survival in patients with metastatic breast cancer, ovarian cancer, and other solid cancers (37, 38). While biologics that sequester Tie2 ligands Ang1 or Ang2 may find clinical utility, there are additional ligands, including Ang4, which activate Tie2 receptors and escape capture by Ang1/Ang2 sequestering biologics (39, 40). Additionally, extracellular signals, including integrins (41, 42) and lysyl oxidase (43, 44), may also activate Tie2-mediated signaling and internalized Tie2 signals to the DNA damage response (44). A selective small molecule inhibitor of Tie2 kinase would be capable of intercepting all of the above activating mechanisms, including those not blocked by the Ang-sequestering biologics.

Herein we report the effects of rebastinib, a potent and selective picomolar inhibitor of the Tie2 receptor tyrosine kinase that inhibits kinase activity by an allosteric "switch control" mechanism, on mammary tumor progression. The goals of this study were to evaluate the cellular effects of rebastinib on both endothelial and macrophage cell populations, its efficacy, both as a single agent and in combination with chemotherapy, in cancer models characterized by Tie2$^+$ macrophage involvement, and to further characterize the *in vivo* effects on myeloid cell composition and vascularization in the tumor microenvironment.

Materials and Methods

Cell lines

CHO-K1 (year of purchase, 2009), EA.hy926 (2012), and HUVECs (various lots from 2012 to 2015) were purchased from the ATCC. All cell lines were cultured as recommended by the supplier, unless otherwise indicated. Media reagents were purchased from Life Technologies or Lonza, Inc. CHO and EA.hy926 cell lines were expanded upon receipt and then frozen at an early passage number in aliquots in liquid N_2. Cells were then passaged fewer than 6 months after resuscitation. HUVECs were passaged <10 times upon resuscitation. The ATCC performs STR analysis for characterization. Further STR characterization on CHO-K1 and EA.hy926 was not performed. *Mycoplasma* testing was performed on a monthly basis for all cell lines (except primary cells such as HUVECs), using the MycoAlert Detection Kit from Lonza, Inc.

Tie2 kinase assay and determination of inhibitor potency

Kinase activity was determined by following the production of ADP from the kinase reaction through coupling with the pyruvate kinase/lactate dehydrogenase system as detailed in Supplementary Data. Percent inhibition values were obtained by comparison of reaction rates with DMSO controls. IC_{50} values were calculated from a series of percent inhibition values determined at a range of inhibitor concentrations using Prism software (GraphPad). Using this pyruvate kinase/lactate dehydrogenase assay, various concentrations of rebastinib were added to an assay mixture. The dissociation rate constant, k_{off}, was calculated as detailed in Supplementary Data.

Crystallization, data collection, and structure refinement of rebastinib with Tie2

Rebastinib was provided by Deciphera Pharmaceuticals. Purified Tie2 (808-1124) crystals were grown as detailed in Supplementary Data. Diffraction data of Tie2-rebastinib crystals were collected at the Advanced Light Source (ALS) Beamline 5.0.1 at a wavelength of 0.9774 Å using an ADSC Q310r detector. Data were reduced with XDS and scaled to 2.05 Å resolution using XSCALE (45). Tie2-rebastinib crystallizes in space group P4(1) with unit cell dimensions $a = b = 63.81$ Å, $c = 177.45$, $\alpha = \beta = \gamma = 90°$ with two molecules in the asymmetric unit. The structure was solved using PHASER (46) and the PDB entry 2008 (47) as the search model. The model was completed with COOT (48) and refined with REFMAC5 (49) using ligand restraint generated with JLigand (50) and one TLS group per chain to Rwork = 0.148 and Rfree = 0.166. Data set and refinement statistics are summarized in Supplementary Table S1.

Western blot assays

Tie2^{hi} iBMM were generated by immortalizing mouse bone marrow macrophages with an SFFV.TAG.WPRE lentivector, as described (51), and by transducing a mouse Tie2 cDNA under the control of a human PGK promoter. Western blot assays to detect total and phospho-Tie2 in HUVECs, EA.hy926, and Tie2^{hi} iBMM cells are detailed in the Supplementary Data. Antibodies against phospho-Tie2 Tyr992 (catalog #4221) and rabbit IgG (HRP-conjugated; catalog #7074) were obtained from Cell Signaling Technology. The antibody against total Tie2 (catalog #sc-324) was obtained from Santa Cruz Biotechnology, Inc.

HUVEC transwell migration assay

Human umbilical vein endothelial cells (HUVEC; Corning 354151) were maintained in EGM medium (Lonza CC-3124) and used within the first 6 passages for transwell assays detailed in Supplementary Data.

Published OnlineFirst August 24, 2017; DOI: 10.1158/1535-7163.MCT-17-0241

Mice

All studies involving mice were carried out in accordance with the National Institutes of Health regulation concerning the care and use of experimental animals and with the approval of the Animal Care and Use Committee of Molecular Imaging, Inc., an AAALAC accredited facility or with the approval by the Albert Einstein College of Medicine Animal Care and Use Committee. Transgenic mice expressing the Polyoma Middle T (PyMT) oncogene under the control of the mammary tumor virus long terminal repeat (MMTV-LTR) were bred in house at the Albert Einstein College of Medicine and maintained on the FVB background.

Transgenic male C57Bl6/6J/RIP1-Tag2 mice heterozygous for the oncogene were bred with wild-type females. Pups were genotyped for the SV40 large TAg by Transnetyx (http://www.transnetyx.com). Starting from 12 weeks of age, RIP1-Tag2 mice were maintained on a sucrose-enriched diet and monitored daily. All procedures involving RIP1-Tag2 mice were performed according to protocols approved by the Veterinary Authorities of the Canton Vaud according to the Swiss Law (license 2574 and 2574/a).

PyMT syngeneic breast cancer implant model

Female FVB/NJ mice (JAXWEST:RB05) were implanted in the fourth mammary fat pad on the left side with 1 million cells in serum-free media that had been dissociated from tumor fragments from MMTV-PyMT donor mice. Treatments began on day 31 when the mean tumor burden for all groups in the experiment was 843 mg or on day 52 when the mean tumor burden for all groups in the experiment was 930 mg as detailed in Supplementary Data. For the eribulin survival study in combination with rebastinib, treatments began on day 42 when the mean tumor burden for all groups in the experiment was 889 mg. Primary tumors were resected on day 45 when the mean tumor burden for the vehicle group was 1,288 mg. Study progression and necropsy for all cohorts are detailed in the Supplementary Data.

Quantification of the F4/80$^+$ and Tie2$^+$ percent area staining. After F4/80 and Tie2 immunostaining, whole slides were digitized on a Pannoramic P250 Flash II digital whole slide scanner at 20× magnification. Digital slides were then analyzed in Visiomorph DP (Visiopharm) with a custom developed app specific to mammary gland morphology, as detailed in the Supplementary Data.

Labeling of tumor vasculature and extravasation of 155 kDa dextran-TMR and measuring circulating tumor cells (CTC). One hour before the termination of the experiments with rebastinib, 3 μg of 155 kDa TMR-dextran was administered by tail vein i.v. to label sites of vascular permeability. In addition, CTCs were isolated from anesthetized mice from blood drawn from the right ventricle of the heart and scored. Both were done as described previously (7) and detailed in Supplementary Data.

Immunofluorescence. Tumor sections were prepared and stained as described previously (7) and detailed in Supplementary data. The following primary antibodies were used for immunostaining of mouse tumor tissues: rat anti-mouse CD68 (clone FA-11, Serotec), or AlexaFluor647-conjugated CD68 (eBioscience), mouse anti-Mena (NBP1-87914, Novus Biologicals), rat anti-ZO-1 (clone R40.76, Millipore), rabbit anti-CD31 (77699s; Cell Signaling Technology), rat anti-Tie2 (16-5987-82; eBioscience), rabbit anti-Iba1 (019-19741; Wako). Sections were washed with PBS-T, and the primary antibodies were detected with AlexaFluor488, 555, or 647 secondary antibody conjugates (Molecular Probes/Invitrogen) and nuclei stained with 4,6-diamidino-2-phenylindole (DAPI).

TMEM immunohistochemistry. Tumor sections were prepared, stained, and quantified as previously described (32).

FACS analysis

The diverse immune cell populations infiltrating vehicle- or rebastinib-treated PyMT tumors were compared by FACS-based quantification. PyMT tumors were surgically isolated, enzymatically digested and resulting single cell suspensions were stained for flow cytometry analysis. Only viable cells (Indo-1-violet^{negative}) were selected for further analysis from a single-cell population, which was initially sorted based on forward scattering (FSC) to exclude clustered cells. The immune cell compartment of all tumors was then gated based on CD45 expression, while lymphocyte versus non-lymphocyte populations were further discriminated based on side scattering (SSC) of CD45$^+$ cells. A gating strategy was then used in the lymphocyte compartment with quantify selective subpopulations, including cytotoxic T-cells (CD45$^+$CD8$^+$), T-helper (CD45$^+$CD4$^+$), T- regulatory (Treg; CD45$^+$CD4$^+$FoxP3$^+$CD25$^+$), and natural killer (NK) cells (CD45$^+$CD335$^+$). A gating strategy was used in the nonlymphocyte compartment with quantify the myeloid-derived suppressor cells (MDSC; CD45$^+$Cd11b$^+$Ly6G$^+$Ly6C$^+$Gr1$^+$), as well as macrophages (CD45$^+$CD11b$^+$F4/80$^+$Gr1$^-$). Further gating strategy was deployed to identify M2 macrophage polarization (CD45$^+$CD11b$^+$F4/80$^+$Gr1$^-$MRC1$^+$) in the macrophage population. Furthermore, Tie2 expression was quantified in both the entire (CD45$^+$CD11b$^+$F4/80$^+$Gr1$^-$MRC1$^+$) and the M2-only macrophage subpopulation (CD45$^+$CD11b$^+$F4/80$^+$Gr1$^-$CD206$^+$MRC1$^+$). The entire gating strategy is outlined in Supplementary Fig. S1.

RIP1-Tag2 transgenic mouse model

Male RIP1-Tag2 mice (11.5- to 12.5-week-old) were treated daily by oral gavage with rebastinib at 10 mg/kg or vehicle control 0.4% HPMC for 4 weeks. Before euthanasia, the mice were retro-orbitally injected with FITC-labeled lectin (to reveal perfused blood vessels). Pancreata and livers were harvested at necropsy for analysis. Immunofluorescence staining, lectin labeling of vasculature imaging and quantification of the RIP1-Tag2 (PNET) model is detailed in the Supplementary Data. To quantify liver micrometastases in PNET bearing mice livers were harvested and fixed overnight in 4% PFA solution at 4°C. The left lobe of each liver was dissected, processed and embedded in optimal cutting temperature compound, as described for pancreata. Analysis of cryosections is detailed in the Supplementary Data.

In vitro intravasation (iTEM) assay

The iTEM assay was performed as described previously (52, 53) and detailed in the Supplementary Data. Transwells were imaged using a Leica SP5 confocal microscope using a 60 × 1.4 numerical aperture objective and processed using ImageJ (NIH) and IMARIS programs. Quantitation was performed by counting the number of tumor cells that had crossed the endothelium within the same field of view (60×, 10 random fields).

Published OnlineFirst August 24, 2017; DOI: 10.1158/1535-7163.MCT-17-0241

Plasma Ang2 levels in rebastinib-treated patients

Post-dose (C_{max}) and pre-dose trough plasma samples on cycle 1 day 8 and pre-dose trough plasma samples on cycle 1 day 22 were analyzed for levels of Ang2 and rebastinib concentration detailed in the Supplementary Data.

Statistical analysis

Individual animals in each cohort are presented as individual points on a dot plot. A horizontal line indicates the mean value, and the error bars represent the standard error of the mean. Statistical significance was determined by the comparison of the means of two groups using an unpaired, two-sided *t* test using Prism (Graph Pad Inc.). Data sets were checked for normality (D'Agostino–Pearson omnibus normality test or Shapiro–Wilk normality test) and unequal variance using Prism (Graph Pad Inc.). Welch's correction was applied to *t* tests as needed. *P* values of less than 0.05 were deemed statistically significant.

Results

X-ray cocrystal structure of rebastinib with Tie2 kinase exhibits unique attributes of Type II switch control binding

A cocrystal structure of rebastinib was obtained in complex with the unphosphorylated human Tie2 kinase domain (residues K808–A1124) at 2.05 Å resolution (Supplementary Table S1; Fig. 1A and B and Supplementary Fig. S2A and S2B). Analysis revealed a Type II binding mode in which rebastinib induces Tie2 into a DFG-out inactive enzymatic conformation, making key interactions with regions of the activation loop

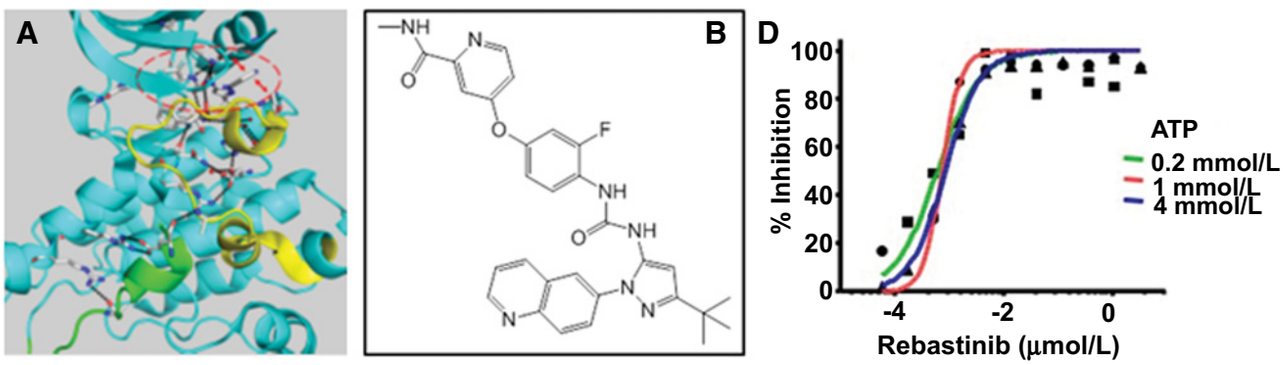

C

Assay	IC_{50} (nmol/L)
Tie2 Kinase	0.63 ± 0.08
Tie2 Kinase, off rate	k*off* = 0.0012 min^{-1}; $t_{1/2}$ = 10 h
HUVEC Cell	0.058 ± 0.033
EA.hy926 Cell	0.091 ± 0.080
IBMM Tie2hi Macrophage	0.26 ± 0.05
Tie2-Expressing CHO cell	2.0 ± 1.7
Ang1-Stimulated HUVEC migration	0.022 ± 0.011

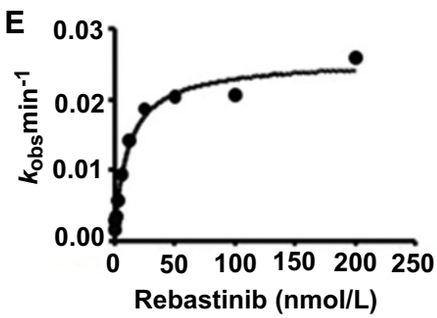

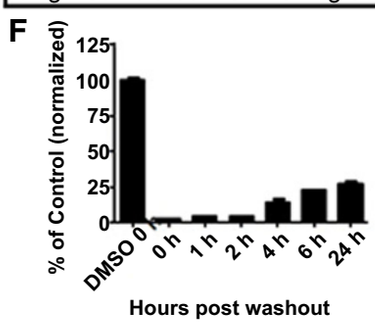

G

Target protein	Kinase	IC_{50} (nmol/L)	Fold-selectivity for TIE2
HUVEC pTIE2	TIE2	0.058	-
SK-N-SH pTRKA	TRKA	0.17	3
SK-N-SH pTRKB	TRKB	0.42	7
3T3 ETV6/TRKC pTRKC	TRKC	2.7	47
K562 pBCR-ABL	BCR-ABL	3.6	62
MV-4-11 pFLT3	FLT3	4.1	71
Recombinant enzyme	~300 others	-	>100

Figure 1.

Rebastinib selectively inhibits the receptor tyrosine kinase Tie2. **A,** Cocrystal structure of rebastinib bound to the Tie2 kinase domain. **B,** Chemical structure of rebastinib. **C,** Inhibition of Tie2 kinase activity with rebastinib in biochemical and cellular assays, where k_{off} is the kinetic constant for rebastinib dissociation from Tie2 and $t_{1/2}$ is the half-life of the rebastinib–Tie2 complex. **D,** Dose response inhibition of Tie2 ATP-dependent kinase activity with rebastinib at indicated concentrations of ATP. **E,** Forward kinetic analysis of rebastinib inhibition of Tie2 activity, where $k_{obs}$is the rate constant for achieving equilibrium inhibition. **F,** Sustained inhibition of Tie2 phosphorylation in CHO cells by rebastinib (1 μmol/L) at indicated time after removal of rebastinib. **G,** Table of nearest kinases inhibited with rebastinib.

Published OnlineFirst August 24, 2017; DOI: 10.1158/1535-7163.MCT-17-0241

conformation-controlling *switch* (yellow ribbon, Fig. 1A), regions of Tie2 which serve as the *cognate switch pocket* (dashed red oval, Fig. 1A), and the ATP hinge region.

For Tie2 conformational activation, the switch is required to bind into its cognate switch pocket. Rebastinib outcompetes the switch for binding into this pocket. Thus, in Fig. 1A and B, rebastinib is shown to occupy the Tie2 switch pocket (dashed red oval), and the activating switch (yellow) is displaced into an inactive conformation, precluding the ability of Tie2 to activate. An annotated description of molecular interactions of rebastinib with Tie2 is shown in Supplementary Fig. S2A and S2B. Rebastinib binding outcompetes the switch by the inhibitor t-butyl moiety (A) displacing switch residue Phe983 (labeled as 1). The fluoro-phenyl ring of the inhibitor (B) additionally stabilizes Phe983 in this inactive state through π-stacking interactions. Inhibitor urea moiety (D) forms hydrogen bonds with both the conserved catalytic salt bridge Glu872 (9)/Lys855 (10) and the switch residue Asp982 (6). This binding modality further nucleates a hydrogen bonding network comprising residues His962, Asp964, Arg968, Asn969, Asp982, and Gly984 (residues 2–7), collapsing these residues into an inactive conformational state incompatible with enzymatic shuttling of phosphate from ATP to a protein substrate. A unique electrostatic π-stacking interaction is formed between switch residue Arg987 (8), the inhibitor quinolinyl ring (C) and Glu872 (9), highlighted with double-tipped red arrows. In composite, rebastinib directly forms 5 hydrogen bonds with Tie2, with overall binding further nucleating an additional 25 hydrogen bonds inducing the switch, switch pocket, and catalytic residues into an inactive state. The hydrogen bond network additionally is consistent with stabilizing the C-terminal inhibitory motif (green) in position for occluding the substrate binding pocket of Tie2. This conformational state of Tie2 induced by rebastinib is incapable of loading a protein substrate or ATP cofactor and provides structural determinants of the picomolar potency of rebastinib (Fig. 1C). Biophysical thermal melt studies also confirmed potent binding of rebastinib to Tie2, resulting in a ΔTM of 14.9C versus apo-Tie2 (Supplementary Fig. S3A–S3C).

Biochemical inhibition of Tie2 and prolonged off-rate

In biochemical assays, rebastinib demonstrated subnanomolar potency as an inhibitor of recombinant human unphosphorylated Tie2 kinase (IC_{50} = 0.63 nmol/L, Fig. 1C). This IC_{50} exceeded the limit of further titration based on the concentration of Tie2 required for the assay. Rebastinib retained subnanomolar potency at adenosine triphosphate (ATP) concentrations as high as 4 mmol/L (Fig. 1D). Rebastinib was found to slowly dissociate from Tie2, yielding a dissociation rate constant (k_{off}) value of 0.0012/minutes (Fig. 1C and E). The $t_{1/2}$ value associated with this k_{off} value for recovery of kinase activity was approximately 10 hours for unphosphorylated Tie2 (Fig. 1C).

In assays with a more complex cellular environment using human umbilical vascular endothelial cells (HUVEC) or EA.hy926 cells, which express Tie2, rebastinib inhibited Ang1-stimulated Tie2 kinase activity with IC_{50} values of 0.058 and 0.091 nmol/L, respectively (Fig. 1C and Supplementary Fig. S4A–S4D). In bone marrow–derived murine macrophages transduced to express Tie2 kinase (IBMM $Tie2^{Hi}$), rebastinib inhibited Tie2 phosphorylation with an IC_{50} value of 0.26 nmol/L (Fig. 1C and Supplementary Fig. S4E and S4F). In a functional chemotaxis assay, rebastinib inhibited Ang1-mediated migration of HUVECs with an IC_{50} of 0.022 nmol/L (Fig. 1C and Supplementary Fig. S5A and S5B). Finally, in transiently transfected Chinese Hamster Ovary (CHO) cells overexpressing constitutively phosphorylated Tie2, rebastinib inhibited Tie2 activity with an IC_{50} value of 2.0 nmol/L (Fig. 1C). Rebastinib demonstrated a prolonged off rate (>24 hours) against Tie2 kinase in transfected CHO cells after inhibitor washout (Fig. 1F).

Rebastinib was evaluated in a panel of 300 human kinases, confirming its selectivity as a Tie2 inhibitor (Supplementary Table S2 and Fig. 1G). TRKA was identified as the nearest neighbor kinase inhibited by rebastinib (Supplementary Table S2). The cellular IC_{50} for inhibition of TRKA phosphorylation by rebastinib was 0.17 nmol/L, which is 3-fold higher than the IC_{50} of Tie2. Related kinases TRKB and TRKC exhibited IC_{50} values of 0.42 nmol/L and 2.74 nmol/L, respectively, showing lesser inhibition by rebastinib. BCR–ABL and FLT3 inhibition by rebastinib were even less potent with IC_{50} values 62- and 71-fold, respectively. Rebastinib has previously been shown to inhibit the BCR–ABL fusion oncoprotein (54). Because rebastinib is approximately 62-fold more selective in binding to Tie2 than BCR–ABL, the effect of rebastinib as a selective Tie2 inhibitor has been further examined in mammary carcinoma and pancreatic neuroendocrine tumors (PNET).

Other marketed, clinical stage, or preclinical compounds have been reported to inhibit Tie2 kinase. Supplementary Table S4 lists these representative agents, including Met inhibitors cabozantinib, foretinib, MGCD265 (glesatinib), crizotinib; BCR-ABL inhibitor ponatinib; ALK/RON inhibitor crizotinib; and other Tie2 inhibitors pexmetinib, and the preclinical tool compound SKB-Tie2. Rebastinib is 17–5,672-fold more potent than these comparator inhibitors (column 3, Supplementary Table S4) for inhibiting Tie2. Moreover, rebastinib is the most selective and potent Tie2 inhibitor versus these comparator compounds (columns 4–14, Supplementary Table S4). By way of example, rebastinib is 7,017-fold more potent for Tie2 versus Met, compared with cabozantinib, foretinib, and MGCD265, all of which exhibit inverse selectivity of less than 1-fold, indicating preferential potency for Met. Rebastinib and SKB-Tie2 are the only inhibitors in Supplementary Table S4, which inhibit Tie2 as their primary target, and rebastinib is 5,672 times more potent than SKB-Tie2 for inhibiting Tie2.

Rebastinib inhibits mammary carcinoma growth and extends mouse survival

To examine rebastinib inhibition of Tie2 signaling *in vivo,* we used the orthotopic mouse mammary cancer implant model in which the polyoma middle T antigen is under the control of the mouse mammary tumor virus long terminal repeat (MMTV-PyMT; refs. 55, 56). PyMT tumors exhibit histology similar to human luminal breast cancer and progress to metastasis (57). Further, PyMT tumors assemble TMEM, the vascular doorway structures associated with tumor cell intravasation and dissemination in mouse mammary tumors and human breast cancer patients, which contain $Tie2^{Hi}$/Vegf-A^{Hi} macrophages (7, 32, 34, 58).

Rebastinib significantly reduced primary tumor growth by 75% and, more importantly, when used in combination with paclitaxel, rebastinib had an additive effect in reducing tumor growth by 90% of control (Fig. 2A). Eribulin, like paclitaxel, is an inhibitor of microtubules and is approved for the treatment of

Published OnlineFirst August 24, 2017; DOI: 10.1158/1535-7163.MCT-17-0241

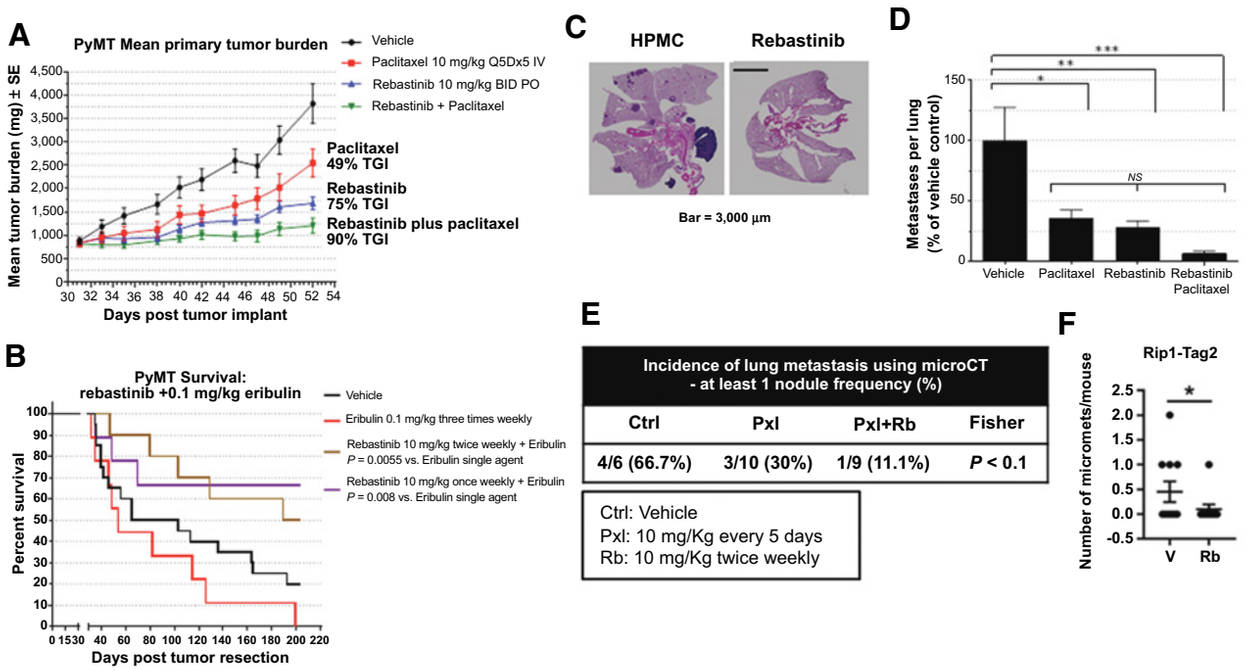

Figure 2.

Rebastinib blocks primary tumor growth, inhibits metastatic growth and extends survival in combination with chemotherapy. **A,** Mean tumor burden in mice with implanted PyMT tumors in the mammary fat pad and treated with vehicle (black line), paclitaxel alone (red line), rebastinib alone (blue line), or rebastinib and paclitaxel in combination (green line). **B,** Intermittent treatment of PyMT mice with rebastinib extends overall survival in combination with eribulin, following the excision of the primary tumor. Primary mammary tumors were resected on day 42, and treatment was begun on day 45. Dosing was continued for 27 weeks and animals followed for survival. **C,** H&E staining of lung tissue from PyMT-bearing mice for lung metastases (vehicle-treated, left; rebastinib-treated, right). **D,** Quantification of area of lung metastases by H&E in the lungs of animals as compared with the vehicle control for the indicated treatments after 3 weeks of treatment. $P < 0.05$ for all relative to vehicle control. **E,** Incidence of lung metastases (nodules) determined by μCT in mice at 9 weeks of treatment. **F,** Rebastinib decreases PNET metastasis to liver, as shown in the Rip1–Tag2 mouse model. HPMC $n = 11$, rebastinib $n = 10$. *, $P < 0.05$.

relapse of refractory metastatic breast cancer. Rebastinib was evaluated in a postsurgical (adjuvant) setting in the PyMT model in combination with eribulin after primary mammary tumor resection (Fig. 2B). In the absence of the primary tumor, the duration of animal survival is a result of overall systemic tumor burden (primarily lung metastases). Eribulin single agent afforded a median survival of 54 days post tumor resection (red curve), less than median survival of 84 days in the vehicle cohort (black curve). Eribulin in combination with rebastinib extended survival of mice to at least 196 to 200 days, depending on the rebastinib dosing schedule (Fig. 2B). Together, these data demonstrate that rebastinib treatment in PyMT mammary tumors either daily, or through intermittent dosing alone or in combination with chemotherapy, reduces primary tumor volume and extends survival time.

Rebastinib reduces lung metastases in mammary carcinoma and liver metastasis in PNETs

Tie2$^+$ macrophages are known to support tumor cell dissemination and metastasis in mammary carcinomas (7, 8, 59). Given that lung is the most frequent site of distant metastasis in breast cancer, we hypothesized that inhibition of Tie2$^+$ macrophage-mediated dissemination by rebastinib would reduce tumor cell metastasis to the lung. Indeed, in orthotopic PyMT tumors, rebastinib was found to reduce the formation of lung metastases alone by 72% and in combination with paclitaxel by 93% (Fig. 2C and D). Given the efficacy of intermittent dosing of rebastinib in extending survival and reducing lung metastases, the effect of rebastinib in combination with paclitaxel therapy on metastasis was evaluated in the PyMT model by microCT (Supplementary Fig. S6). As shown (Fig. 2E), there was a difference ($P < 0.1$) in the incidence of lung metastasis afforded by the combination of paclitaxel with rebastinib dosed twice weekly at 10 mg/kg compared with chemotherapy-treated or vehicle-treated mice.

Unlike PyMT mammary carcinoma, daily oral dosing of rebastinib at 10 mg/kg for 4 weeks did not detectably inhibit the growth of pancreatic insulinomas in the transgenic RIP1-Tag2 model of PNET (60; Supplementary Fig. S7). However, we evaluated rebastinib for inhibition of liver metastases. According to a late treatment protocol targeting established PNETs, 11–12-week-old male RIP1-Tag2 mice were treated for 4 weeks with rebastinib and liver micrometastasis were quantified at termination. Rebastinib significantly inhibited liver metastases by 75% compared with control (Fig. 2F).

Rebastinib reduces Tie2$^+$ macrophages and microvessel density in mammary carcinoma and PNETs

Tie2$^+$ macrophages have been associated with tumor angiogenesis, tumor cell dissemination, and metastasis (10–12). Because treatment with rebastinib reduced metastasis to the lungs

Published OnlineFirst August 24, 2017; DOI: 10.1158/1535-7163.MCT-17-0241

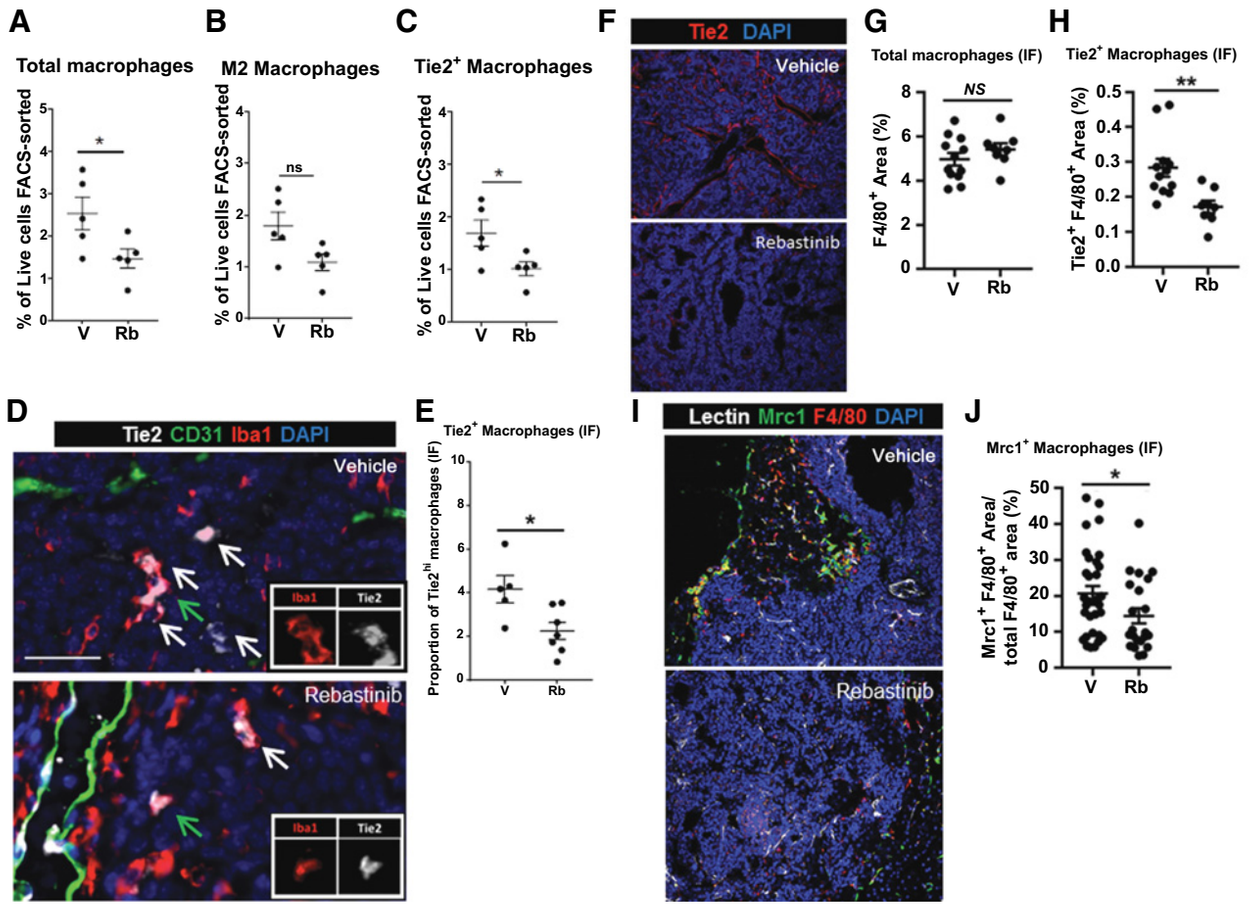

Figure 3.

Rebastinib reduces Tie2$^+$ macrophage infiltration and microvessel density in mammary carcinoma and PNETs. **A–C,** FACS analysis of whole PyMT mammary tumors and their associated stroma, treated with either vehicle (v, $n = 5$) or rebastinib (Rb, $n = 5$). **A,** Total macrophages, (**B**) M2 macrophages, (**C**) Tie2$^+$ macrophages as a percentage of all cells in the tumor tissue and its associated stroma. **D,** Multichannel immunofluorescence (IF) microscopy of PyMT sections stained for Iba1 (macrophages), CD31 (blood vessels), and Tie2. Arrows indicate cells that are double positive for Iba1 and Tie2, i.e., Tie2$^+$ macrophages. Magnified inset shows representative Tie2$^+$/Iba1$^+$ cells depicted with the green arrow in each figure. Bar, 40 um. **E,** Quantification of Tie2$^+$ macrophages shown in **D** in PyMT tumors from (V) control and (Rb) rebastinib treated mice. *, $P < 0.05$. **F,** IF staining of Tie2 in Rip1-Tag2 PNET in animals treated with vehicle (v) or rebastinib (Rb). **G,** Quantification of total F4/80$^+$ macrophages in PNET tumors treated with rebastinib (Rb) or vehicle (v). *ns*, nonsignificant. **H,** Quantification of F4/80$^+$/Tie2$^+$ macrophages in PNET tumor tissue as a percentage of tissue area. Vehicle $n = 12$, rebastinib $n = 8$ for **G** and **H**. **, $P = 0.0051$. Rebastinib at 10 mg/kg, orally daily. **I,** IF microscopy of PNET tumor sections stained for perfused blood vessels (lectin), macrophages (F4/80), and Mrc1. **J,** Quantification of Mrc1$^+$/F4/80$^+$ macrophages at invasive front of PNET tumor sections from **I** in animals treated with vehicle (v) or rebastinib (Rb). Each dot represents one image acquired at 200× magnification. Vehicle $n = 9$, rebastinib $n = 7$. *, $P < 0.05$. Rebastinib at 10 mg/kg, orally twice weekly.

in the PyMT mammary carcinoma and liver metastasis in the PNET model, we sought to investigate the effects of rebastinib on cell infiltration into the tumor and, in particular, Tie2$^+$ macrophage infiltration. FACs sorting of whole PyMT mammary tumors and their associated peripheral stroma showed that rebastinib significantly decreased both total and Tie2$^+$ macrophages (Fig. 3A–C) but did not significantly affect lymphoid immune cell composition (Supplementary Fig. S8). There was a trend toward reduction of M2-polarized macrophages (Fig. 3B) and the subset of M2 macrophages expressing Tie2 (Supplementary Fig. S8); however, this reduction did not achieve significance. In a separate analysis, multichannel Immunofluorescence (IF) staining (Iba1 for macrophages, CD31 for endothelium and Tie2) was used to specifically distinguish the Tie2$^+$ macrophage subpopulation (Fig. 3D and E) and demonstrated that the Tie2$^+$ macrophage subpopulation was significantly decreased in response to rebastinib treatment (Fig. 3D and E and Supplementary Fig. S9A), confirming the reduction in the Tie2$^+$ macrophage subpopulation in response to rebastinib, as also determined by FACs analysis (Fig. 3C).

In the PNET model, there was a decrease in Tie2 staining in response to rebastinib (Fig. 3F), but rebastinib did not affect the total macrophage infiltrate (F4/80$^+$ area; Fig. 3G). However, rebastinib significantly decreased intratumoral Tie2$^+$ macrophages (Fig. 3H) and led to a significant decrease in protumoral Mrc1$^+$ F4/80$^+$ macrophages at the tumor invasive front (Fig. 3I and J).

Taxane-based chemotherapies, such as paclitaxel, mobilize bone marrow–derived mesenchymal and endothelial progenitors,

Published OnlineFirst August 24, 2017; DOI: 10.1158/1535-7163.MCT-17-0241

and CD11b$^+$ myeloid cells, including Tie2$^+$ monocytes, into the primary tumor microenvironment (49–57). Tie2$^+$ monocyte progenitors are known to transform into Tie2$^+$ macrophages, which associate with newly constructed tumor blood vessels and promote tumor regrowth (20, 58, 59). The effects of paclitaxel on the presence of Tie2$^+$ macrophages and microvessel density were examined in PyMT tumors, either untreated or treated with rebastinib. First, we found that paclitaxel significantly increased both total macrophages and Tie2$^+$ macrophages (Fig. 4A and B). Furthermore, we found that rebastinib, selectively decreased Tie2$^+$ macrophage infiltration occurring in response to paclitaxel (Fig. 4A and B).

Second, paclitaxel treatment of mice with PyMT mammary tumors increased CD31$^+$ microvessel density (MVD) over vehicle-treated animals (Fig. 4C and D). When treated with rebastinib, in combination with paclitaxel, MVD was reduced to significantly below HPMC (vehicle control) levels, similar to MVD in mice with rebastinib treatment alone (Fig. 4C and D). These results indicate that paclitaxel increases both microvessel density and Tie2$^+$ macrophages in PyMT tumors, while rebastinib counteracts the paclitaxel-induced increases of both. In addition, rebastinib reduced the density of perfused (i.e., functional) blood vessels in PNET (Fig. 4E and F), thus showing antiangiogenic effects in two independent mouse tumor models.

The association of pericytes with tumor blood vessels promotes vascular maturation and decreases vascular permeability and metastasis (61). Rebastinib increased vascular maturation in the remaining vessels in the PNET model, as shown by the higher proportion of pericyte-covered, Ng2$^+$ blood vessels (Supplementary Fig. S9B and S9C). Thus, in both mammary carcinomas and PNETs, rebastinib induced vascular phenotypes that were consistent with decreases in permeability, cancer cell dissemination, and metastasis.

Tie2 inhibition with rebastinib inhibits TMEM-mediated vascular permeability and tumor cell intravasation in mammary carcinoma

Because rebastinib exhibited efficacy in the reduction of primary tumor burden (Fig. 2), Tie2$^+$ macrophage infiltration in primary tumors (Fig. 3) and lung metastases after administration of intermittent doses (Fig. 2), we investigated if rebastinib inhibits Tie2$^+$ macrophage function specifically at TMEM sites, where tumor cell intravasation and dissemination in mammary tumors occur.

TMEM density was not affected by Tie2 inhibition with rebastinib using a 10 mg/kg twice weekly intermittent dosing regimen (Fig. 5A and B). However, inhibition of Tie2 signaling with rebastinib reduced TMEM-mediated changes in vascular permeability and the number of CTCs as compared with vehicle control (Fig. 5C–E). In particular, staining of vascular ZO-1 (vascular integrity) increased and extravascular dextran (vascular permeability) decreased at TMEM after administration of rebastinib, indicating that vascular junctions were stabilized, reducing vascular permeability at TMEM (Fig. 5C, D and F). Although total TMEM density was not affected (Fig. 5A and B), TMEM function was impaired as quantified by the ratio of extravascular dextran to vascular ZO-1 (Fig. 5G), consistent with a decrease in Tie2$^+$ macrophage function in TMEM. Interestingly, the effects of rebastinib on TMEM function *in vivo* phenocopied the genetic ablation of macrophages in the MaFIA mouse (11).

Rebastinib inhibits macrophage-dependent transendothelial migration *in vitro*

Due to the role of Tie2$^+$ macrophages in vascular permeability and tumor cell intravasation at TMEM *in vivo* (Fig. 6A; ref. 7), we studied whether inhibition of Tie2 with rebastinib would impair TMEM–mediated tumor cell transendothelial migration *in vitro*. We studied this by using the previously established *in vitro* TMEM-dependent subluminal-to-luminal transendothelial migration (intravasation) assay (Fig. 6B; refs. 52, 53). We found that rebastinib significantly inhibits macrophage-dependent transendothelial migration of breast cancer cells in the intravasation direction with an IC_{50} between 50 and 100 pmol/L, and to background levels observed in the absence of macrophages (TC alone) at 500 pmol/L (Fig. 6C, left).

To determine if the Tie2$^+$ macrophages are the cells inhibited by rebastinib in this assay, the intravasation assay was conducted using the complete dose–response evaluation of rebastinib but in the absence of macrophages. When the Tie2$^+$ macrophages were selectively excluded from the intravasation assay, rebastinib had no effect on tumor cell intravasation at any concentration (Fig. 6C, right). The requirement of macrophage-specific Tie2 expression for TMEM-mediated transendothelial tumor cell migration was demonstrated by using murine macrophages in the intravasation assay that expressed either low or high levels of Tie2 (Supplementary Fig. S10). As shown in Fig. 6D, using macrophages expressing high levels of Tie2 (Tie2^{Hi}) resulted in a greater than 4-fold increase in tumor cell transendothelial migration compared with background (Bg), whereas using macrophages expressing low levels of Tie2 (Tie2^{Lo}) did not support such a large increase. Rebastinib treatment ablated transendothelial migration induced by the Tie2^{Hi} macrophages (Fig. 6D). Collectively, these data indicate that Tie2 signaling in TMEM-associated macrophages is required for tumor cell transendothelial migration. These data also demonstrate that inhibition of Tie2 in the intravasation assay selectively impairs Tie2^{Hi} macrophages and does not impair endothelial monolayer integrity.

Furthermore, inhibition of TrkA, the nearest-neighbor kinase inhibited by rebastinib (Fig. 1G), using the selective TrkA inhibitor entrectinib ($IC_{50} = 130$ pmol/L), had no effect on tumor cell transendothelial migration in either the presence or absence of macrophages, indicating that the inhibition seen with rebastinib was not due to off-target effects involving TrkA (Supplementary Table S3 and Fig. 6E). Additionally, rebastinib had no effect on tumor cell proliferation at the concentrations used in these studies, nor did rebastinib affect tumor cell transendothelial migration in the absence of macrophages, ruling out a direct effect of rebastinib on tumor cells in the intravasation assay (Supplementary Fig. S11).

Rebastinib therapy results in an Ang2 biomarker readout in human patients

In order to clinically evaluate Tie2 inhibition, Ang2 levels were examined in 20 consented patients from a first-in-human phase I chronic myelogenous leukemia (CML) and acute myelogenous leukemia (AML) study (NCT 00827138) before and after treatment with 100 or 150 mg twice weekly rebastinib (Fig. 7). Clinically, compensatory elevations in circulating growth factor ligands is observed upon inhibition of their cognate receptor tyrosine kinases, including Vegf/Vegfr2,

Published OnlineFirst August 24, 2017; DOI: 10.1158/1535-7163.MCT-17-0241

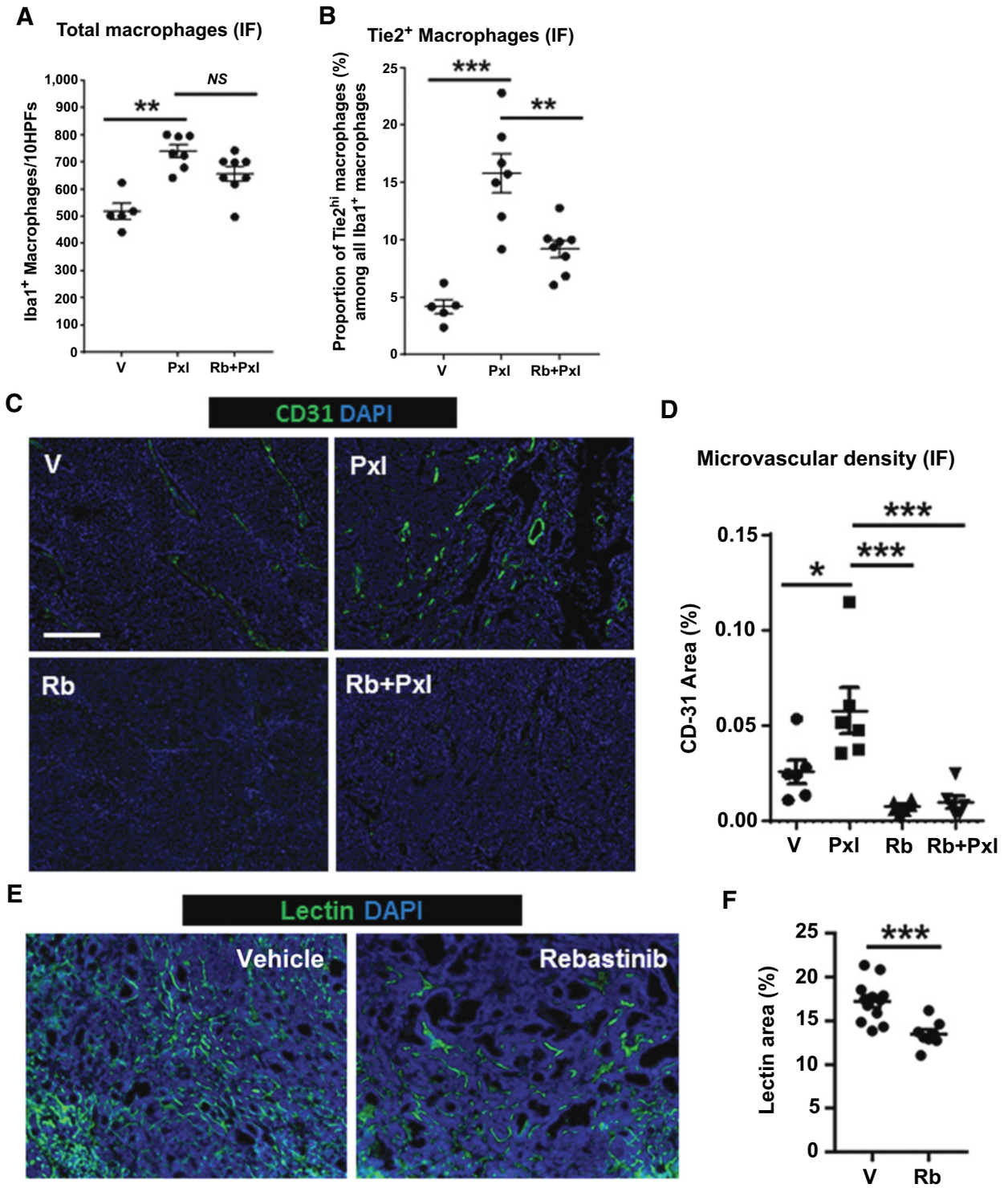

Figure 4.

Rebastinib reduces paclitaxel-induced increases in Tie2$^+$ macrophages and microvessel density. **A,** Quantification of total macrophages and **B,** Tie2$^+$ macrophages in PyMT tumors in response to control (V), paclitaxel (Pxl), and rebastinib + paclitaxel (Rb + Pxl). **C,** IF staining of vasculature with CD31 (green) in PyMT tumors in mice treated with the vehicle and drug combinations shown. Bar, 50 μm. **D,** Quantification of microvessel density as a percentage of area from CD31 staining shown in **C** *, $P < 0.05$; **, $P < 0.01$; ***, $P < 0.0005$. **E,** IF staining of vasculature with lectin (green) in PNET tumors treated with vehicle or rebastinib. **F,** Quantification of microvessel density as a percentage of perfused lectin area from tumor tissue stained in **E** showing that rebastinib significantly reduces vascular density in PNET. Each dot is a mouse in which multiple tumors were analyzed. HPMC $n = 12$, rebastinib $n = 8$. ***, $P = 0.0008$. Paclitaxel at 10 mg/kg i.v., every five days ($n = 10$); rebastinib at 10 mg/kg orally, daily.

Published OnlineFirst August 24, 2017; DOI: 10.1158/1535-7163.MCT-17-0241

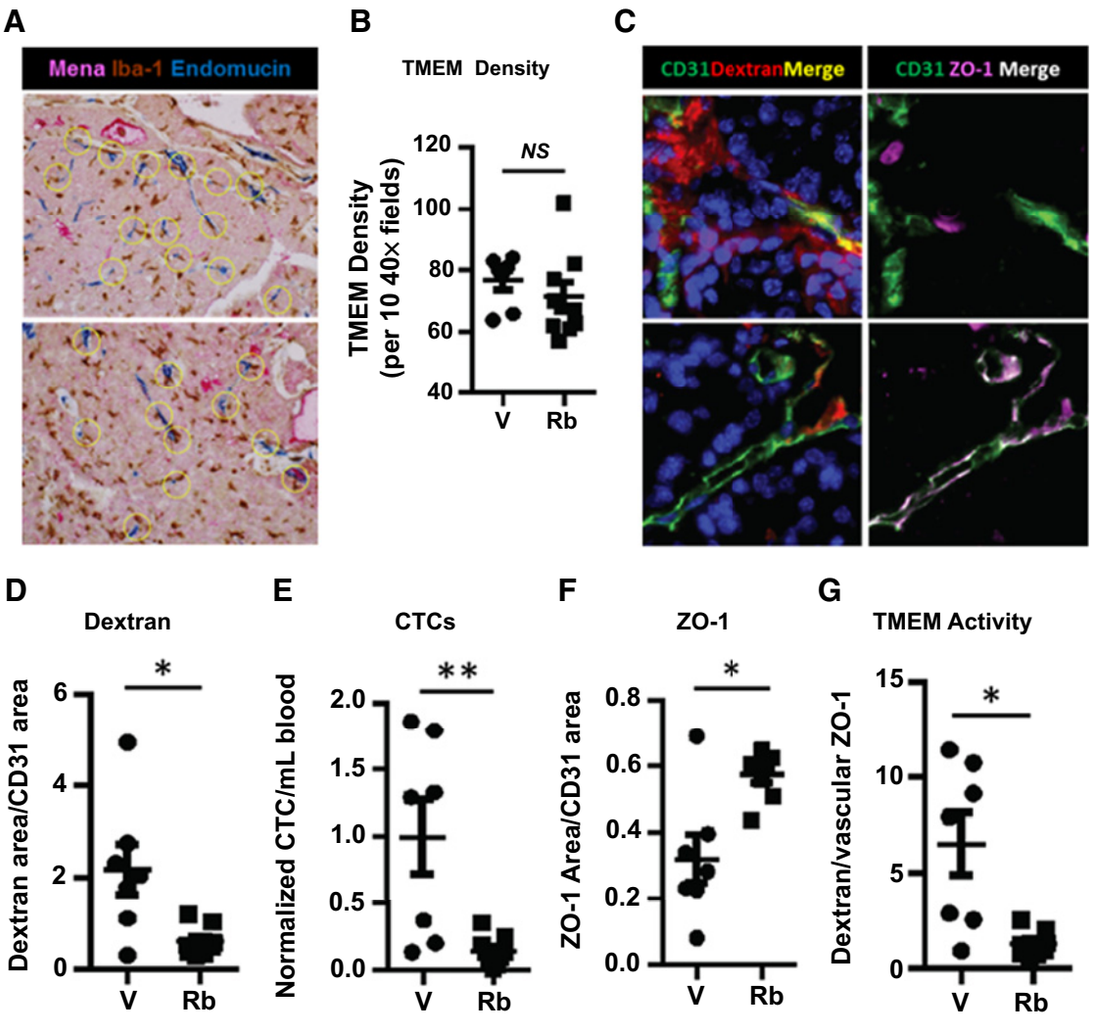

Figure 5.

Inhibition of Tie2 with rebastinib impairs TMEM function and tumor cell dissemination in PyMT mammary carcinoma. **A,** IHC staining of tumors for TMEM before and after treatment with rebastinib. Vasculature (endomucin, blue), Mena overexpressing tumor cells (Mena, pink) and macrophages (Iba1, brown). TMEM are circled. **B,** Quantification of TMEM density in 10 high-power fields (HPFs; no significant difference). **C,** IF imaging of tumor sections. Tumors are stained for blood vessel endothelial cells (CD31), vascular perfusion/leakage (155 kDa dextran-TMR), cell nuclei (DAPI), or endothelial junctions (ZO-1). **D–G**, Vehicle or treatment with 10 mg/kg rebastinib both for twice weekly for 3 weeks. **D,** Extravascular 155 kDa dextran-TMR (vehicle, $n = 7$; rebastinib $n = 9$; *, $P = 0.042$). **E,** Normalized quantification of CTCs (**, $P = 0.004$). **F,** Vascular ZO-1 staining intensity relative to CD31 staining (*, $P = 0.0124$). **G,** Quantification of TMEM activity as extravascular dextran relative to ZO-1 staining intensity (vehicle, $n = 7$; rebastinib $n = 9$; *, $P = 0.0177$). All panels: V, vehicle control; Rb, rebastinib.

Csf1/Csf1R, and others (62, 63). Thus, the effect of rebastinib on compensatory increases in circulating angiopoietin levels secondary to Tie2 inhibition was evaluated. On day 22 after starting rebastinib treatment, increases in Ang2 were observed in 19 of 20 patients, no change was observed in one patient, and a >2-fold increase in Ang2 plasma levels was observed in 14 of 20 (70%) patients. The average fold increase for all 20 patients was 2.6 ± 1.2 SD. To assess whether changes in plasma levels of Ang2 were correlated with plasma levels of rebastinib, data were fit to linear regression models. Both C_{max} (Supplementary Fig. S12A) and trough exposures of rebastinib on day 8 (Supplementary Fig. S12B) significantly correlated with increased levels of plasma Ang2. Increased plasma Ang levels also correlated with trough rebastinib exposures on day 22 (Supplementary Fig. S12C).

Discussion

Here, we report that rebastinib is a novel switch control inhibitor of Tie2 tyrosine kinase with picomolar potency for blocking Tie2 enzymatic and cellular activity in endothelial cells and TEMs and exhibits efficacy in malignant mammary carcinoma and PNETs. In mammary tumors, Tie2 blockade by rebastinib results in inhibition of tumor growth, invasion, and metastasis. Examination of the effects of rebastinib at the cellular level demonstrates that rebastinib reduced tumor

Published OnlineFirst August 24, 2017; DOI: 10.1158/1535-7163.MCT-17-0241

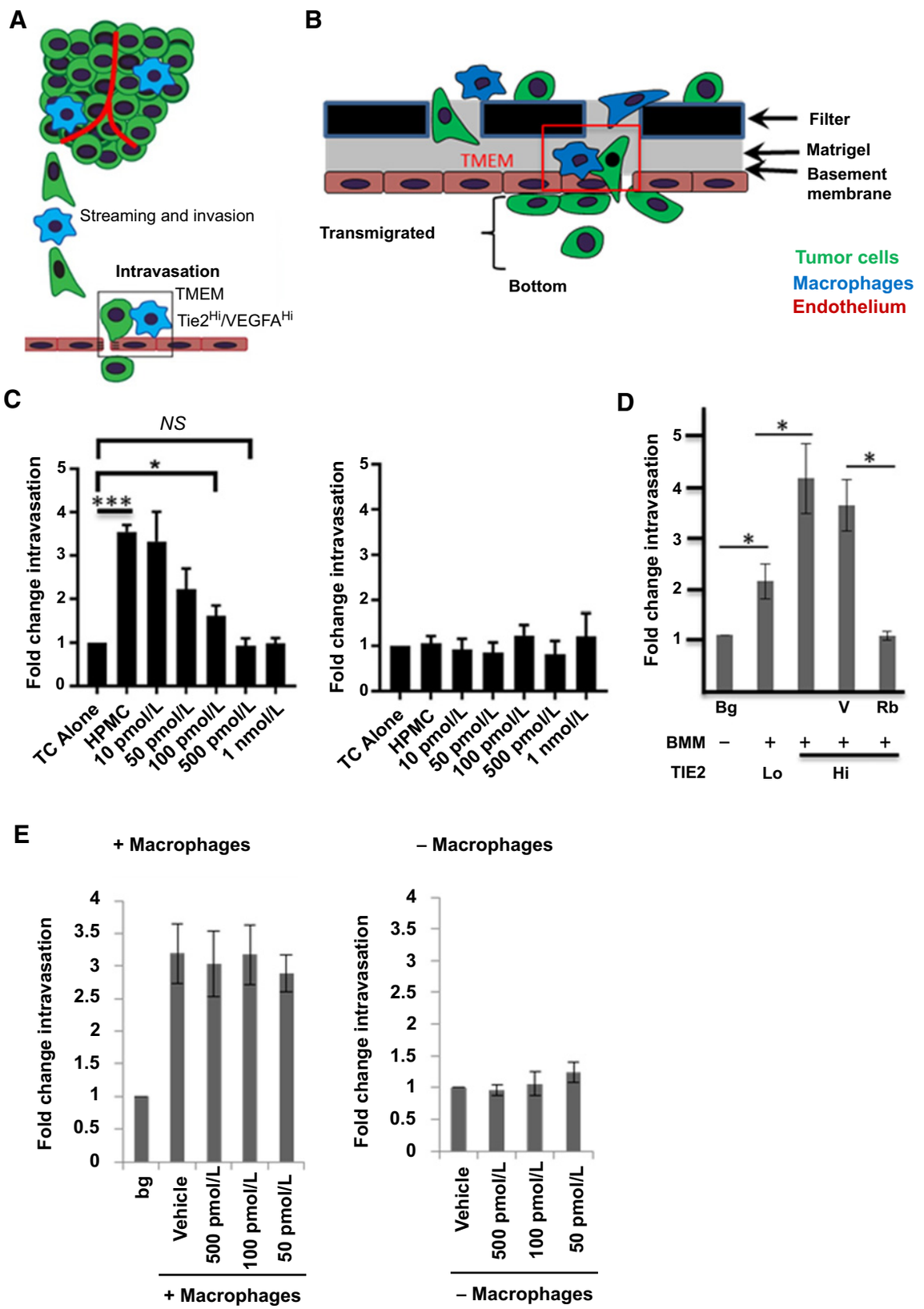

Published OnlineFirst August 24, 2017; DOI: 10.1158/1535-7163.MCT-17-0241

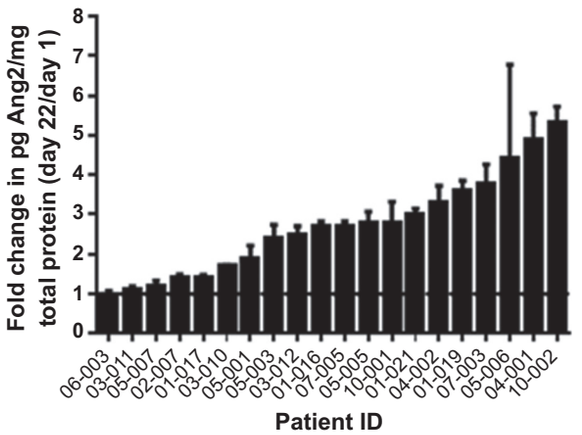

Figure 7.

Angiopoietin-2 plasma levels in 20 patients from the first-in-human phase I CML and AML study (NCT 00827138) who received rebastinib. For subjects who signed appropriate informed consent documents, C_{max} and trough plasma levels of rebastinib on cycle 1 day 8 and trough plasma samples on cycle 1 day 21 were correlated with levels of Ang2 determined on the same day as the pharmacokinetic (PK) sampling, where available. Fold change in individual patient Ang2 plasma levels at day 22 versus baseline pretreatment Ang2 value at day 1. The average fold increase for all 20 patients was 2.6 $\pm$ 1.2 SD.

vascular density, and Tie2$^+$ macrophages in the PyMT mammary tumor and its stroma. However, rebastinib did not lead to a change in immune cell composition beyond the changes observed in Tie2$^+$ macrophages. Though the mechanism of such decreased Tie2 expression is not clear, we speculate that the cross-activation of Tie2 by endothelial integrins (41) can be potentially blocked by rebastinib-mediated inhibition of Tie2, further leading to downregulation of the Tie2 receptor from the cell surface. Tie2 internalization has also been reported after ionizing radiation therapy, indicating that other treatment modalities can also mediate Tie2 downregulation (43).

We noticed that rebastinib treatment significantly reduced the general macrophage population in the PyMT mouse model of breast cancer, but not in the transgenic mouse model of PNET, Rip1-Tag2 (Fig. 3A and G). Importantly, however, the intratumoral Tie2$^+$ macrophages were reduced in both animal models tested (Fig. 3C and H), indicating that rebastinib affects the dynamics of specific macrophage subpopulations in the primary tumor microenvironment in a context-dependent manner, thus without necessarily affecting the total macrophage population, as also evidenced by radiotherapy, chemotherapy, or other drug treatments (24, 27, 64, 65). In addition, in PyMT tumors, although TMEM density was not decreased by rebastinib, TMEM function was dramatically impaired by rebastinib effects on Tie2$^+$ macrophages, as evidenced by decreased vascular permeability, CTCs, and metastasis *in vivo*, and decreased TMEM-associated transendothelial migration *in vitro*. The effects of rebastinib are further elevated when combined with paclitaxel or eribulin treatment in mice at least in part because rebastinib significantly inhibits the recruitment of Tie2$^+$ macrophages in response to paclitaxel, thereby affecting microvessel density and TMEM assembly.

Rebastinib is a potent picomolar inhibitor of Tie2 kinase that inhibits by an allosteric "switch control pocket" mechanism. Analysis of the cocrystal structure of rebastinib with Tie2 revealed a Type II binding mode in which rebastinib induces Tie2 into a DFG-out inactive enzymatic conformation, making key interactions with regions of the conformation-controlling switch, with regions of Tie2 that serve as the cognate switch pocket, and with the kinase hinge region. This binding mode engenders picomolar potency for rebastinib inhibition of Tie2 biochemically and in cellular macrophage and endothelial assays. Cellular potencies for inhibiting murine Tie2 (macrophage assays: IC_{50} values ~0.075 to 0.26 nmol/L) and human Tie2 (endothelial cell assays: IC_{50} values ~0.058 to 0.91 nmol/L) are comparable, consistent with the high interspecies identity (99%) with only 3 differences out of 355 residues in the kinase domain (Supplementary Fig. S13). The Tie2 kinase binding mode of rebastinib results in a long-dissociation off rate ($t_{1/2}$ = 10 hours).

Tie2$^+$ macrophages are a subset of highly skewed protumoral macrophages in the tumor microenvironment that are elevated following treatment with chemotherapy, antiangiogenic agents, or vascular disrupting agents that render tumors hypoxic (6, 8, 9, 15). Tie2$^+$ macrophage recruitment contributes to evasive revascularization and invasion in these hypoxic tumors (66). Perivascular Tie2$^+$ macrophages have been shown to participate in the doorways for intravasation of tumor cells called TMEM (7, 32, 34, 52). Administration of rebastinib to orthotopic models of mammary carcinoma and PNETs resulted in reduced vascular density, reduced Tie2$^+$ macrophages, and

Figure 6.

Rebastinib inhibits macrophage-mediated tumor cell intravasation *in vitro*. **A,** Schematic diagram of TMEM-mediated tumor cell intravasation in breast tumors. Tumor cells (green) and macrophages (blue) comigrate (called streaming) to TMEM where tumor cells cross the endothelium (pink). **B,** The *in vitro* intravasation assay drawn approximately to scale where the bottom of a transwell is coated with Matrigel and a sealed HUVEC endothelial monolayer is allowed to mature so that it is impermeable to dextran diffusion and has high electrical resistance. Tumor cells (green) and macrophages (blue) are added to the top of the transwell (the tissue/abluminal side). The dimensions of the assay were determined using optical sectioning with a confocal microscope. Tumor cells undergo transendothelial migration in the intravasation direction at sites of endothelium associated macrophages. **C,** left, Fold change in the number of tumor cells that transmigrate the HUVEC monolayer in the presence of Bac1.25 mouse macrophages (vehicle and with increasing concentrations of rebastinib); TC alone, background activity when tumor cells are without macrophages. Right, Same as left except all in the absence of macrophages. Note that rebastinib has no effect on background levels of tumor cell transendothelial migration in the absence of macrophages. **D,** Fold change in the number of tumor cells that transmigrate the HUVEC monolayer in the presence of iBMM with spontaneous endogenous Tie2 (Tie2^{Lo}) expression, Tie2-overexpressing (Tie2^{Hi}) iBMMs (see Supplementary Fig. S8 for relative expression levels), and in the presence of Tie2^{Hi} iBMMs treated with vehicle (V) or 500 pmol/L rebastinib (Rb). Bg, background, tumor cells alone. *, $P < 0.05$; ***, $P < 0.005$. **E,** TrkA inhibition with entrectinib has no effect on tumor cell intravasation *in vitro*. Fold change in the number of tumor cells that transmigrate the HUVEC monolayer in the intravasation assay in the presence of macrophages (left: control and with increasing concentrations of entrectinib; bg, background, tumor cells alone) and absence of macrophages (right).

Published OnlineFirst August 24, 2017; DOI: 10.1158/1535-7163.MCT-17-0241

TMEM function. In addition to efficacy as an antivascular agent, rebastinib reduces the proangiogenic Tie2$^+$ macrophage population in the tumor microenvironment, limiting revascularization and tumor growth. In contrast to other antivascular agents, rebastinib has the potential to not only decrease tumor volume in combination with chemotherapy, but may also prevent Tie2$^+$ macrophage–mediated tumor regrowth and increased TMEM function, leading to metastasis. This is further supported by the evidence that rebastinib reduces tumor cell invasion, dissemination, and metastasis in both the PyMT and RIP1-Tag2 models of invasive and metastatic cancers, and reverses paclitaxel-induced increased intratumoral Tie2$^+$ macrophages and eribulin-induced reduction in survival secondary to lung metastases in the PyMT model.

The finding that rebastinib suppresses the infiltration of Tie2$^+$ macrophages into tumors raises secondary questions involving how rebastinib limits recruitment of Tie2$^+$ macrophages and how the function of isolated Tie2$^+$ macrophages may be altered in response to rebastinib. Recent studies have shown that local vascular endothelial production of Ang2 recruits Tie2$^+$ macrophages to the tumor indicating that inhibition of Ang2 stimulation of the Tie2 receptor on macrophages by rebastinib is involved in suppressing Tie2$^+$ macrophage recruitment (67). Furthermore, recent studies have shown that the inhibition of Vegf production by, or its release from, Tie2$^+$ macrophages blocks their ability to support angiogenesis-dependent tumor relapse (9) and tumor cell dissemination by TMEM (7).

Mechanistically, tumor cell dissemination in mammary carcinoma occurs exclusively at Tie2^{Hi}/Vegf-A^{Hi} TMEM sites. Motile tumor cells cross the endothelium when Tie2^{Hi}/Vegf-A^{Hi} macrophages in TMEM locally dissolve vascular junctions through Vegf-A signaling (7). Rebastinib impaired TMEM function in vivo, resulting in reduced vascular permeability and tumor cell intravasation, and a corresponding dramatic decrease in CTCs. Decreased tumor cell intravasation from the primary tumor prevented tumor cell metastasis, explaining the decrease in metastatic lung nodules with rebastinib treatment and further supporting the potential impact of rebastinib in preventing Tie2$^+$ macrophage-mediated tumor metastasis. It is also noted that the effects of rebastinib *in vivo* for inhibiting TMEM function phenocopy macrophage ablation in the MaFIA mouse and selective gene knockout ablation of Vegf in Tie2$^+$ perivascular macrophages (7).

The observation that rebastinib specifically inhibits the Tie2^{Hi} macrophages in TMEM, thereby inhibiting tumor cell intravasation has been further confirmed in the *in vitro* assay replicating transendothelial tumor cell migration at TMEM. In the presence of 0.5 nmol/L rebastinib, tumor cell intravasation was reduced to background levels of tumor cell intravasation as measured in the absence of macrophages. No effect of rebastinib on tumor cell transendothelial migration was demonstrated in the absence of macrophages, indicating a specific effect on macrophages and no effect of rebastinib on either tumor cell or endothelial cell components of this assay. Furthermore, incorporation of Tie2$^+$ macrophages into the intravasation assay led to a significant increase in tumor cell transendothelial migration compared with macrophages with lower Tie2 expression. Rebastinib reversed the enhanced tumor cell migration induced by Tie2$^+$ macrophages. Collectively, these results support a significant role of Tie2$^+$ macrophages in transendothelial migration and demonstrate that rebastinib specifically blocks Tie2$^+$ macrophages in TMEM which impairs an essential mechanism in tumor cell intravasation and metastasis in mammary carcinoma that is unique to TMEM.

Although the studies included herein demonstrate the potent antiangiogenic and antimacrophage properties of rebastinib to blunt tumor growth, invasiveness, metastasis, and improve survival in murine cancer models, it is also known that the angiopoietin–Tie2 signaling axis is immunosuppressive and blockade of this axis could also provide the potential to favorably modulate cancer treatment outcomes via reversal of Tie2 signaling cross-talk to the adaptive immune system. Tie2$^+$ macrophages have been shown to release IL10 and thereby suppress CD8$^+$ cytotoxic T cells, expand immunosuppressive Tregs, and cause dendritic cell anergy (22, 29). It has also been reported that in long-term responding subjects treated with anti-CTLA4 agents, a humoral reaction is generated against angiopoietins (68). Dual blockade of Ang2 and Vegf-A has been demonstrated to induce an antiangiogenic effect that facilitated extravasation and perivascular accumulation of activated, IFN-γ expressing cytotoxic T lymphocytes in various tumor models, and therapeutic benefit was enhanced by combination with PD-1 blockade (69). Recently, it has also been reported that circulating Ang2 levels are predictive and prognostic for treatment outcomes in melanoma patients treated with checkpoint inhibitors. High pretreatment circulating Ang2 was associated with reduced overall survival in patients treated with CTLA4 and PD-1 checkpoint therapies. Ang2 expression was associated with increased CD163$^+$ macrophage tumor infiltration and Ang2 increased PDL-1 expression on M2-polarized macrophages (67).

Clinical effects of rebastinib on Ang2 plasma levels were evaluated in a recently completed first-in-human phase I trial in CML patients (70). Although not a solid tumor clinical study, during the course of this first-in-human trial, informed consent was obtained from 22 patients to explore treatment versus baseline values of circulating Ang2 as a readout of Tie2 target engagement. Rebastinib treatment led to a significant compensatory increase in Ang2, indicative of systemic Tie2 inhibition. Because Ang2 is primarily secreted from endothelial cells lining the vasculature, it is likely that this Tie2 response is due to endothelial cell inhibition of Tie2 by rebastinib. These results indicate that changes in circulating levels of Ang2 may provide a circulating biomarker of rebastinib-induced Tie2 inhibition in future solid tumor trials.

There is now compelling evidence for Ang2 to function as a (partial) Tie2 agonist in tumor angiogenesis (71). This is also supported by the finding that Ang2 is upregulated in many tumor types, including breast cancer, and its levels may indeed exceed those of Ang1 (4, 72–74). In these contexts (high Ang2/low Ang1), Ang2 may function as a Tie2 activator (75). Therefore, we reason that decreasing Tie2 activity in tumors (e.g., by rebastinib) may phenocopy the effects of Ang2 blockade. We and others have shown that Ang2 blockade in several cancer models, including MMTV-PyMT mice, leads to decreased tumor angiogenesis, which is associated with the "normalization" of the remaining blood vessels (2, 8, 69, 76). Therefore, our finding that Tie2 inhibition increases pericyte coverage of the tumor blood vessels (a parameter of vascular normalization) is consistent with the expected outcome of blocking the Ang2–Tie2 axis in an angiogenic microenvironment. This is particularly true in the presence of Vegf-A, which prevents more profound vascular pruning in the absence of Ang2. The increase in serum Ang2 after

rebastinib may be consistent with the upregulation of Ang2 that occurs after selective Ang2 blockade. Indeed, in previous studies it has been reported that Ang2 blockade dramatically increases *Ang2* transcription (2, 71). Because the inhibition of Tie2 may phenocopy, at least partly, Ang2 blockade, rebastinib may similarly elicit Ang2 upregulation in tumor-bearing hosts, yet still block Ang2 signaling due to its profound picomolar potency for arresting Tie2 in a Type II inactive state. The elevation of circulating Ang2 levels in patients treated with rebastinib is consistent with this hypothesis (Fig. 7).

In the current study, we described the preclinical validation for the use of rebastinib in two animal models; breast carcinoma (PyMT) and PNET. As rebastinib is intended for use in human patients, we have recently demonstrated in another study (77) the effects of rebastinib on breast cancer patient-derived xenografts. Rebastinib mediated suppression of TMEM-dependent dissemination, with or without the presence of neoadjuvant chemotherapy. Based on data presented in the Karagiannis and colleagues (2017) study (77) along with the current study, rebastinib has now been approved (currently in phase Ib) for a clinical trial in breast cancer patients (NCT02824575). Taken together, rebastinib is a promising therapy for the treatment of solid carcinomas, characterized by prominent Tie2$^+$ macrophage presence in the tumor microenvironment.

Disclosure of Potential Conflicts of Interest

B.D. Smith, C.B. Leary, M.D. Kaufman, W.-P. Lu, G. Al-Ani, and D.L. Flynn have ownership interest (including patents) in Deciphera Pharmaceuticals. J.S. Condeelis is a consultant/advisory board member for Deciphera. No potential conflicts of interest were disclosed by the other authors.

Disclaimer

Views and opinions of, and endorsements by the authors, do not reflect those of the U.S. Army or the Department of Defense.

Authors' Contributions

Conception and design: A.S. Harney, G.S. Karagiannis, J. Pignatelli, B.D. Smith, M. De Palma, D.L. Flynn, J.S. Condeelis

Development of methodology: A.S. Harney, G.S. Karagiannis, J. Pignatelli, B.D. Smith, E. Kadioglu, W.-P. Lu, D. Entenberg, L. Chun, M. De Palma, J.G. Jones, J.S. Condeelis

Acquisition of data (provided animals, acquired and managed patients, provided facilities, etc.): A.S. Harney, J. Pignatelli, B.D. Smith, E. Kadioglu, M.M. Hood, C.B. Leary, W.-P. Lu, G. Al-Ani, X. Chen, L. Chun, M. De Palma, J.G. Jones, D.L. Flynn

Analysis and interpretation of data (e.g., statistical analysis, biostatistics, computational analysis): A.S. Harney, G.S. Karagiannis, J. Pignatelli, B.D. Smith, E. Kadioglu, C.B. Leary, W.-P. Lu, G. Al-Ani, D. Entenberg, L. Chun, M. De Palma, J.G. Jones, D.L. Flynn, J.S. Condeelis

Writing, review, and/or revision of the manuscript: A.S. Harney, G.S. Karagiannis, B.D. Smith, E. Kadioglu, M.D. Kaufman, D. Entenberg, M.H. Oktay, M. De Palma, J.G. Jones, D.L. Flynn, J.S. Condeelis

Administrative, technical, or material support (i.e., reporting or organizing data, constructing databases): B.D. Smith, S.C. Wise, M.D. Kaufman, Y. Wang

Study supervision: B.D. Smith, S.C. Wise, M. De Palma, D.L. Flynn, J.S. Condeelis

Other (initial discovery and characterization of rebastinib): S.C. Wise

Grant Support

This research was funded by Deciphera Pharmaceuticals, LLC, the Department of Defense Breast Cancer Research Program under award number (W81XWH-13-1-0010 A.S. Harney and W81XWH-14-1-0286 J. Pignatelli), NIH CA100324, CA150344, CA013330-44S3, S10 OD019961, and the Integrated Imaging Program at Albert Einstein College of Medicine.

The costs of publication of this article were defrayed in part by the payment of page charges. This article must therefore be hereby marked *advertisement* in accordance with 18 U.S.C. Section 1734 solely to indicate this fact.

Received March 17, 2017; revised July 12, 2017; accepted August 10, 2017; published OnlineFirst August 24, 2017.

References

1. Saharinen P, Eklund L, Pulkki K, Bono P, Alitalo K. VEGF and angiopoietin signaling in tumor angiogenesis and metastasis. Trends Mol Med 2011;17:347–62.
2. Rigamonti N, Kadioglu E, Keklikoglou I, Wyser Rmili C, Leow CC, De Palma M. Role of angiopoietin-2 in adaptive tumor resistance to VEGF signaling blockade. Cell Rep 2014;8:696–706.
3. Eroglu Z, Stein CA, Pal SK. Targeting angiopoietin-2 signaling in cancer therapy. Expert Opin Investig Drugs 2013;22:813–25.
4. Sfiligoi C, de Luca A, Cascone I, Sorbello V, Fuso L, Ponzone R, et al. Angiopoietin-2 expression in breast cancer correlates with lymph node invasion and short survival. Int J Cancer 2003;103:466–74.
5. Maisonpierre PC, Suri C, Jones PF, Bartunkova S, Wiegand S, Radziejewski C, et al. Angiopoietin-2, a natural antagonist for Tie2 that disrupts in vivo angiogenesis. Science 1997;277:55–60.
6. Gabrusiewicz K, Liu D, Cortes-Santiago N, Hossain MB, Conrad CA, Aldape KD, et al. Anti-vascular endothelial growth factor therapy-induced glioma invasion is associated with accumulation of Tie2-expressing monocytes. Oncotarget 2014;5:2208–20.
7. Harney AS, Arwert EN, Entenberg D, Wang Y, Guo P, Qian BZ, et al. Real-time imaging reveals local, transient vascular permeability, and tumor cell intravasation stimulated by TIE2hi macrophage-derived VEGFA. Cancer Discov 2015;5:932–43.
8. Mazzieri R, Pucci F, Moi D, Zonari E, Ranghetti A, Berti A, et al. Targeting the ANG2/TIE2 axis inhibits tumor growth and metastasis by impairing angiogenesis and disabling rebounds of proangiogenic myeloid cells. Cancer Cell 2011;19:512–26.
9. Hughes R, Qian BZ, Rowan C, Muthana M, Keklikoglou I, Olson OC, et al. Perivascular M2 macrophages stimulate tumor relapse after chemotherapy. Cancer Res 2015;75:3479–91.
10. Piao Y, Park SY, Henry V, Smith BD, Tiao N, Flynn DL, et al. Novel MET/TIE2/VEGFR2 inhibitor altiratinib inhibits tumor growth and invasiveness in bevacizumab-resistant glioblastoma mouse models. Neuro Oncol 2016;18:1230–41.
11. Riabov V, Gudima A, Wang N, Mickley A, Orekhov A, Kzhyshkowska J. Role of tumor associated macrophages in tumor angiogenesis and lymphangiogenesis. Front Physiol 2014;5:75.
12. Ferrara N. VEGF and intraocular neovascularization: from discovery to therapy. Transl Vis Sci Technol 2016;5:10.
13. Jayson GC, Kerbel R, Ellis LM, Harris AL. Antiangiogenic therapy in oncology: current status and future directions. Lancet 2016;388:518–29.
14. Bergers G, Hanahan D. Modes of resistance to anti-angiogenic therapy. Nat Rev Cancer 2008;8:592–603.
15. Welford AF, Biziato D, Coffelt SB, Nucera S, Fisher M, Pucci F, et al. TIE2-expressing macrophages limit the therapeutic efficacy of the vascular-disrupting agent combretastatin A4 phosphate in mice. J Clin Invest 2011;121:1969–73.
16. Cukierman E, Bassi DE. The mesenchymal tumor microenvironment: a drug-resistant niche. Cell Adh Migr 2012;6:285–96.
17. Borriello L, DeClerck YA. [Tumor microenvironment and therapeutic resistance process]. Med Sci 2014;30:445–51.
18. Meads MB, Gatenby RA, Dalton WS. Environment-mediated drug resistance: a major contributor to minimal residual disease. Nat Rev Cancer 2009;9:665–74.
19. Wyckoff J, Wang W, Lin EY, Wang Y, Pixley F, Stanley ER, et al. A paracrine loop between tumor cells and macrophages is required for tumor cell migration in mammary tumors. Cancer Res 2004;64:7022–9.

Published OnlineFirst August 24, 2017; DOI: 10.1158/1535-7163.MCT-17-0241

20. Wyckoff JB, Wang Y, Lin EY, Li JF, Goswami S, Stanley ER, et al. Direct visualization of macrophage-assisted tumor cell intravasation in mammary tumors. Cancer Res 2007;67:2649–56.
21. De Palma M, Venneri MA, Galli R, Sergi Sergi L, Politi LS, Sampaolesi M, et al. Tie2 identifies a hematopoietic lineage of proangiogenic monocytes required for tumor vessel formation and a mesenchymal population of pericyte progenitors. Cancer Cell 2005;8:211–26.
22. Coffelt SB, Chen YY, Muthana M, Welford AF, Tal AO, Scholz A, et al. Angiopoietin 2 stimulates TIE2-expressing monocytes to suppress T cell activation and to promote regulatory T cell expansion. J Immunol 2011;186:4183–90.
23. Liu L, Cash TP, Jones RG, Keith B, Thompson CB, Simon MC. Hypoxia-induced energy stress regulates mRNA translation and cell growth. Mol Cell 2006;21:521–31.
24. Shiao SL, Ruffell B, DeNardo DG, Faddegon BA, Park CC, Coussens LM. TH2-polarized CD4(+) T cells and macrophages limit efficacy of radiotherapy. Cancer Immunol Res 2015;3:518–25.
25. Shree T, Olson OC, Elie BT, Kester JC, Garfall AL, Simpson K, et al. Macrophages and cathepsin proteases blunt chemotherapeutic response in breast cancer. Genes Dev 2011;25:2465–79.
26. Nakasone ES, Askautrud HA, Kees T, Park JH, Plaks V, Ewald AJ, et al. Imaging tumor-stroma interactions during chemotherapy reveals contributions of the microenvironment to resistance. Cancer Cell 2012;21:488–503.
27. DeNardo DG, Brennan DJ, Rexhepaj E, Ruffell B, Shiao SL, Madden SF, et al. Leukocyte complexity predicts breast cancer survival and functionally regulates response to chemotherapy. Cancer Discov 2011;1:54–67.
28. Escamilla J, Schokrpur S, Liu C, Priceman SJ, Moughon D, Jiang Z, et al. CSF1 receptor targeting in prostate cancer reverses macrophage-mediated resistance to androgen blockade therapy. Cancer Res 2015;75:950–62.
29. Ibberson M, Bron S, Guex N, Faes-van't Hull E, Ifticene-Treboux A, Henry L, et al. TIE-2 and VEGFR kinase activities drive immunosuppressive function of TIE-2-expressing monocytes in human breast tumors. Clin Cancer Res 2013;19:3439–49.
30. Dvorak HF, Orenstein NS, Carvalho AC, Churchill WH, Dvorak AM, Galli SJ, et al. Induction of a fibrin-gel investment: an early event in line 10 hepatocarcinoma growth mediated by tumor-secreted products. J Immunol 1979;122:166–74.
31. Karagiannis GS, Goswami S, Jones JG, Oktay MH, Condeelis JS. Signatures of breast cancer metastasis at a glance. J Cell Sci 2016;129:1751–8.
32. Robinson BD, Sica GL, Liu YF, Rohan TE, Gertler FB, Condeelis JS, et al. Tumor microenvironment of metastasis in human breast carcinoma: a potential prognostic marker linked to hematogenous dissemination. Clin Cancer Res 2009;15:2433–41.
33. Oktay MH, Gertler FB, Liu YF, Rohan TE, Condeelis JS, Jones JG. Correlated immunohistochemical and cytological assays for the prediction of hematogenous dissemination of breast cancer. J Histochem Cytochem 2012;60:168–73.
34. Rohan TE, Xue X, Lin HM, D'Alfonso TM, Ginter PS, Oktay MH, et al. Tumor microenvironment of metastasis and risk of distant metastasis of breast cancer. J Natl Cancer Inst 2014;106.
35. Oliner J, Min H, Leal J, Yu D, Rao S, You E, et al. Suppression of angiogenesis and tumor growth by selective inhibition of angiopoietin-2. Cancer Cell 2004;6:507–16.
36. Leow CC, Coffman K, Inigo I, Breen S, Czapiga M, Soukharev S, et al. MEDI3617, a human anti-angiopoietin 2 monoclonal antibody, inhibits angiogenesis and tumor growth in human tumor xenograft models. Int J Oncol 2012;40:1321–30.
37. McConachie A, Newman D, Tucci M, Puckett A, Tsao A, Hughes J, et al. The effect on bioadhesive polymers either freely in solution or covalently attached to a support on human macrophages. Biomed Sci Instrum 1999;35:45–50.
38. Monk BJ, Poveda A, Vergote I, Raspagliesi F, Fujiwara K, Bae DS, et al. Anti-angiopoietin therapy with trebananib for recurrent ovarian cancer (TRINOVA-1): a randomised, multicentre, double-blind, placebo-controlled phase 3 trial. Lancet Oncol 2014;15:799–808.
39. Brunckhorst MK, Wang H, Lu R, Yu Q. Angiopoietin-4 promotes glioblastoma progression by enhancing tumor cell viability and angiogenesis. Cancer Res 2010;70:7283–93.
40. Valenzuela DM, Griffiths JA, Rojas J, Aldrich TH, Jones PF, Zhou H, et al. Angiopoietins 3 and 4: diverging gene counterparts in mice and humans. Proc Natl Acad Sci U S A 1999;96:1904–9.
41. Dalton AC, Shlamkovitch T, Papo N, Barton WA. Constitutive association of Tie1 and Tie2 with endothelial integrins is functionally modulated by angiopoietin-1 and fibronectin. PLoS One 2016;11:e0163732.
42. Cascone I, Napione L, Maniero F, Serini G, Bussolino F. Stable interaction between alpha5beta1 integrin and Tie2 tyrosine kinase receptor regulates endothelial cell response to Ang-1. J Cell Biol 2005;170:993–1004.
43. Mammoto T, Jiang E, Jiang A, Mammoto A. Extracellular matrix structure and tissue stiffness control postnatal lung development through the lipoprotein receptor-related protein 5/Tie2 signaling system. Am J Respir Cell Mol Biol 2013;49:1009–18.
44. Hossain MB, Shifat R, Johnson DG, Bedford MT, Gabrusiewicz KR, Cortes-Santiago N, et al. TIE2-mediated tyrosine phosphorylation of H4 regulates DNA damage response by recruiting ABL1. Sci Adv 2016;2:e1501290.
45. Kabsch W. Xds. Acta Crystallogr D Biol Crystallogr 2010;66:125–32.
46. McCoy AJ, Grosse-Kunstleve RW, Adams PD, Winn MD, Storoni LC, Read RJ. Phaser crystallographic software. J Appl Crystallogr 2007;40:658–74.
47. Hodous BL, Geuns-Meyer SD, Hughes PE, Albrecht BK, Bellon S, Caenepeel S, et al. Synthesis, structural analysis, and SAR studies of triazine derivatives as potent, selective Tie-2 inhibitors. Bioorg Med Chem Lett 2007;17:2886–9.
48. Emsley P, Lohkamp B, Scott WG, Cowtan K. Features and development of Coot. Acta Crystallogr D Biol Crystallogr 2010;66:486–501.
49. Murshudov GN, Skubak P, Lebedev AA, Pannu NS, Steiner RA, Nicholls RA, et al. REFMAC5 for the refinement of macromolecular crystal structures. Acta Crystallogr D Biol Crystallogr 2011;67:355–67.
50. Lebedev AA, Young P, Isupov MN, Moroz OV, Vagin AA, Murshudov GN. JLigand: a graphical tool for the CCP4 template-restraint library. Acta Crystallogr D Biol Crystallogr 2012;68:431–40.
51. Squadrito ML, Baer C, Burdet F, Maderna C, Gilfillan GD, Lyle R, et al. Endogenous RNAs modulate microRNA sorting to exosomes and transfer to acceptor cells. Cell Rep 2014;8:1432–46.
52. Roh-Johnson M, Bravo-Cordero JJ, Patsialou A, Sharma VP, Guo P, Liu H, et al. Macrophage contact induces RhoA GTPase signaling to trigger tumor cell intravasation. Oncogene 2014;33:4203–12.
53. Pignatelli J, Goswami S, Jones JG, Rohan TE, Pieri E, Chen X, et al. Invasive breast carcinoma cells from patients exhibit MenaINV- and macrophage-dependent transendothelial migration. Sci Signal 2014;7:ra112.
54. Chan WW, Wise SC, Kaufman MD, Ahn YM, Ensinger CL, Haack T, et al. Conformational control inhibition of the BCR-ABL1 tyrosine kinase, including the gatekeeper T315I mutant, by the switch-control inhibitor DCC-2036. Cancer Cell 2011;19:556–68.
55. Lin EY, Jones JG, Li P, Zhu L, Whitney KD, Muller WJ, et al. Progression to malignancy in the polyoma middle T oncoprotein mouse breast cancer model provides a reliable model for human diseases. Am J Pathol 2003;163:2113–26.
56. Roussos ET, Wang Y, Wyckoff JB, Sellers RS, Wang W, Li J, et al. Mena deficiency delays tumor progression and decreases metastasis in polyoma middle-T transgenic mouse mammary tumors. Breast Cancer Res 2010;12:R101.
57. Lin EY, Nguyen AV, Russell RG, Pollard JW. Colony-stimulating factor 1 promotes progression of mammary tumors to malignancy. J Exp Med 2001;193:727–40.
58. Newman AC, Hughes CC. Macrophages and angiogenesis: a role for Wnt signaling. Vasc Cell 2012;4:13.
59. De Palma M, Mazzieri R, Politi LS, Pucci F, Zonari E, Sitia G, et al. Tumor-targeted interferon-alpha delivery by Tie2-expressing monocytes inhibits tumor growth and metastasis. Cancer Cell 2008;14:299–311.
60. Hanahan D. Heritable formation of pancreatic beta-cell tumours in transgenic mice expressing recombinant insulin/simian virus 40 oncogenes. Nature 1985;315:115–22.
61. Keskin D, Kim J, Cooke VG, Wu CC, Sugimoto H, Gu C, et al. Targeting vascular pericytes in hypoxic tumors increases lung metastasis via angiopoietin-2. Cell Rep 2015;10:1066–81.
62. Schmitz V, Vilanueva H, Raskopf E, Hilbert T, Barajas M, Dzienisowicz C, et al. Increased VEGF levels induced by anti-VEGF treatment are independent of tumor burden in colorectal carcinomas in mice. Gene Ther 2006;13:1198–205.

Published OnlineFirst August 24, 2017; DOI: 10.1158/1535-7163.MCT-17-0241

63. Ries CH, Cannarile MA, Hoves S, Benz J, Wartha K, Runza V, et al. Targeting tumor-associated macrophages with anti-CSF-1R antibody reveals a strategy for cancer therapy. Cancer Cell 2014;25:846–59.
64. Rebucci M, Michiels C. Molecular aspects of cancer cell resistance to chemotherapy. Biochem Pharmacol 2013;85:1219–26.
65. Elliott LA, Doherty GA, Sheahan K, Ryan EJ. Human tumor-infiltrating myeloid cells: phenotypic and functional diversity. Front Immunol 2017;8:86.
66. Cortes-Santiago N, Hossain MB, Gabrusiewicz K, Fan X, Gumin J, Marini FC, et al. Soluble Tie2 overrides the heightened invasion induced by anti-angiogenesis therapies in gliomas. Oncotarget 2016;7:16146–57.
67. Wu X, Giobbie-Hurder A, Liao X, Connelly C, Connolly EM, Li J, et al. Angiopoietin-2 as a biomarker and target for immune checkpoint therapy. Cancer Immunol Res 2017;5:17–28.
68. Schoenfeld J, Jinushi M, Nakazaki Y, Wiener D, Park J, Soiffer R, et al. Active immunotherapy induces antibody responses that target tumor angiogenesis. Cancer Res 2010;70:10150–60.
69. Schmittnaegel M, Rigamonti N, Kadioglu E, Cassara A, Wyser Rmili C, Kiialainen A, et al. Dual angiopoietin-2 and VEGFA inhibition elicits antitumor immunity that is enhanced by PD-1 checkpoint blockade. Sci Transl Med 2017;9. pii: eaak9670.
70. Cortes J, Talpaz M, Smith HP, Snyder DS, Khoury J, Bhalla KN, et al. Phase 1 dose-finding study of rebastinib (DCC-2036) in patients with relapsed chronic myeloid leukemia and acute myeloid leukemia. Haematologica 2017;102:519–28.
71. Daly C, Eichten A, Castanaro C, Pasnikowski E, Adler A, Lalani AS, et al. Angiopoietin-2 functions as a Tie2 agonist in tumor models, where it limits the effects of VEGF inhibition. Cancer Res 2013;73:108–18.
72. Tsutsui S, Inoue H, Yasuda K, Suzuki K, Takeuchi H, Nishizaki T, et al. Angiopoietin 2 expression in invasive ductal carcinoma of the breast: its relationship to the VEGF expression and microvessel density. Breast Cancer Res Treat 2006;98:261–6.
73. Zhang ZL, Liu ZS, Sun Q. Expression of angiopoietins, Tie2 and vascular endothelial growth factor in angiogenesis and progression of hepatocellular carcinoma. World J Gastroenterol 2006;12:4241–5.
74. Hata K, Nakayama K, Fujiwaki R, Katabuchi H, Okamura H, Miyazaki K. Expression of the angopoietin-1, angopoietin-2, Tie2, and vascular endothelial growth factor gene in epithelial ovarian cancer. Gynecol Oncol 2004;93:215–22.
75. Daly C, Pasnikowski E, Burova E, Wong V, Aldrich TH, Griffiths J, et al. Angiopoietin-2 functions as an autocrine protective factor in stressed endothelial cells. Proc Natl Acad Sci U S A 2006;103:15491–6.
76. Nasarre P, Thomas M, Kruse K, Helfrich I, Wolter V, Deppermann C, et al. Host-derived angiopoietin-2 affects early stages of tumor development and vessel maturation but is dispensable for later stages of tumor growth. Cancer Res 2009;69:1324–33.
77. Karagiannis GS, Pastoriza JM, Wang Y, Harney AS, Entenberg D, Pignatelli J, et al. Neoadjuvant chemotherapy induces breast cancer metastasis through a TMEM-mediated mechanism. Sci Transl Med 2017;9(399), eaan0026.